Terrain Relative Navigation in a Lunar Landing Scenario Using autoNGC

Michael A. Shoemaker*, Sun Hur-Diaz†, Andrew J. Liounis‡, John M. Van Eepoel§, Michael J. Romeo¶, Victoria C. Wu‖, Sarah D. Dangelo**, Noble Hatten††, Lauren G. Schlenker‡‡, Steven P. Hughes§§, Samuel R. Price¶¶, and Luke B. Winternitz***

NASA Goddard Space Flight Center, Greenbelt, MD 20771

NASA Goddard Space Flight Center is developing Autonomous Navigation Guidance and Control (autoNGC) as a flight software system for future onboard use for missions in a variety of orbital regimes, including cislunar space and beyond. This paper describes processor-in-the-loop (PIL) testing using a lunar landing scenario with terrain relative navigation (TRN) and weak-signal GPS. We give an overview of the autoNGC project, and describe preliminary navigation simulation results. We also describe the TRN PIL tests on a flight-like development board, using simulated images rendered from Lunar Reconnaissance Orbit high-resolution digital terrain models. The navigation simulations show that weak-signal GPS combined with TRN during a descent from a low lunar parking orbit results in sufficiently low navigation uncertainties to support such a mission profile independent of ground-based navigation. The PIL tests show that onboard image processing and landmark correlation is achievable at a sufficiently high measurement rate.

I. Introduction

Navigation in cislunar space has traditionally been performed with Earth-based radiometric tracking, but the increasing number of deep space missions reduces the availability of the finite number of tracking assets. A vibrant cislunar economy requires improved onboard navigation capabilities that do not rely exclusively on Earth-based tracking. Autonomous Navigation Guidance and Control (autoNGC) is an internal research and development (IRAD) project at NASA Goddard Space Flight Center (GSFC), begun in FY2019, to provide a multi-mission onboard software platform that integrates and controls spacecraft navigation, guidance, and control hardware and software components. autoNGC was designed to address NASA Technology Taxonomy TX05.4 Network Provided Position, Navigation, and Timing, which desires to "reduce reliance on Earth-based systems for ground-based tracking, ranging, trajectory and orbit determination, and maneuver planning and execution functions"[1]. Solutions to autonomously navigate in cislunar space are increasingly attractive, given NASA's goals with Gateway, Artemis, Commercial Lunar Payload Services (CLPS), LunaNet, and others. The focus of this paper is a description of the terrain relative navigation (TRN) functionality included in autoNGC, and a reporting of the processor-in-the-loop (PIL) testing that has been performed, with emphasis on a lunar landing use case. The autoNGC simulations analyze a vehicle departing a low lunar orbit (LLO) to an altitude near the lunar surface, using measurements from weak-signal Global Positioning System (GPS) and TRN to surface landmarks. The LLO and descent trajectory are in view of the Earth to allow GPS measurement visibility, and the terminal phase of the descent occurs over the sunlit portion of the lunar surface to allow TRN measurements from a passive camera.

Although GPS and other Global Navigation Satellite System (GNSS) signals are tied to the Earth, we can consider them to be a free resource to support autonomous missions in cislunar space that are independent of ground-based

*Aerospace Engineer, Navigation and Mission Design Branch (Code 595), NASA Goddard Space Flight Center, and AIAA Senior Member.
†Aerospace Engineer, Navigation and Mission Design Branch (Code 595), NASA Goddard Space Flight Center.
‡Aerospace Engineer, Navigation and Mission Design Branch (Code 595), NASA Goddard Space Flight Center.
§Aerospace Engineer, Navigation and Mission Design Branch (Code 591), NASA Goddard Space Flight Center.
¶Computer Engineer, Science Data Processing Branch (Code 587), NASA Goddard Space Flight Center.
‖Computer Engineer, Science Data Processing Branch (Code 587), NASA Goddard Space Flight Center.
**Computer Engineer, Science Data Processing Branch (Code 587), NASA Goddard Space Flight Center.
††Aerospace Engineer, Navigation and Mission Design Branch (Code 595), NASA Goddard Space Flight Center.
‡‡Aerospace Engineer, Navigation and Mission Design Branch (Code 595), NASA Goddard Space Flight Center.
§§Aerospace Engineer, Navigation and Mission Design Branch (Code 595), NASA Goddard Space Flight Center.
¶¶Aerospace Engineer, Navigation and Mission Design Branch (Code 596), NASA Goddard Space Flight Center.
***Aerospace Engineer, Navigation and Mission Design Branch (Code 596), NASA Goddard Space Flight Center.

tracking. GPS signals have been used from orbits above the GPS constellations since the 1990s, including more recently on NASA's Magnetospheric Multiscale Mission (MMS), which currently holds the record for the highest operational use of GPS at its initial Phase 1 apogee distance of 76,000 km[2], followed by its current apogee at nearly half the distance to the moon[3]. The use of weak GPS signals at the Moon has also been studied for a number of years[3–6]. Firefly Aerospace will fly the Lunar GNSS Receiver Experiment (LuGRE), a joint NASA and Italian Space Agency payload, aboard the CLPS Task Order 19D flight in 2023[7]. LuGRE is a technology demonstration payload that will receive GPS L1 C/A and L5, and Galileo Open Service E1 and E5a signals, and demonstrate navigation and timing capabilities from an Earth range of 30 to 60 Earth radii, including on the lunar surface.

TRN is another potential measurement type for vehicles operating near the lunar surface. Because the surface of the moon has been mapped with good accuracy from a variety of missions over the years, TRN measurements like line-of-sight bearing measurements to natural surface landmarks represent another source of non-Earth-based navigation measurements. Past and ongoing examples of mission studies and planned capabilities to use TRN measurements to support lunar landers include ALHAT[8], ALTAIR[9], SPLICE[10], and OPAL[11]. Johnson and Montgomery[12] give a useful categorization of different TRN types. TRN measurements in general can include both passive measurements (*e.g.*, camera-based using reflected sunlight) and active measurements (*e.g.*, LIDAR-based); in this paper, we restrict the discussion to passive camera-based systems for use with autoNGC, although future capabilities that incorporate LIDAR systems are in development. Besides the lunar-focused systems described above, other examples of TRN include the Mars 2020 Perseverance lander and OSIRIS-REx. Perseverance used its Lander Vision System[13] to successfully perform in-flight autonomous TRN during Mars entry, descent, and landing. OSIRIS-REx performed autonomous TRN onboard during the asteroid Bennu touch-and-go sampling phase using its Natural Feature Tracking system[14].

Closely related to the TRN methods described above are other optical navigation (OpNav) techniques, which are typically applied when the vehicle is farther away from the target celestial body. OpNav is the process of capturing images of celestial targets (planets, small bodies, natural satellites) against a star background, while the targets are distant and occupy a smaller number of pixels in an image compared with TRN. While not directly applicable to the final stages of a precision lunar landing, autoNGC includes OpNav funcionality, which shares a developmental heritage with our TRN component described in more detail below.

The remainder of this paper gives an overview of the autoNGC architecture, and describes software simulations of some functionality during the high-altitude portions of a lunar lander descent from a LLO towards the the surface. We also describe processor-in-the-loop (PIL) tests of the TRN functionality, to further characterize the expected measurement rate and image processing time on a flight-like processor.

II. autoNGC Architecture

This section describes how autoNGC flight software (FSW) will address this need for autonomous onboard capabilities by integrating together and improving on several existing components, as shown in Figure 1, many having mature flight heritage. Some of the autoNGC components most relevant to the current simulations are discussed in more detail below.

A. Core Flight System

The central hub of the autoNGC architecture is GSFC's open source Core Flight System (cFS)*, which has flown on a number of missions[15]. cFS is a platform- and project-independent reusable software framework and set of reusable software applications having three key aspects: a dynamic run-time environment, layered software, and a component based design. The cFS architecture contains a configurable set of requirements and code that allow cFS to be tailored for each environment including desktop and closed loop simulation environments. A key benefit of cFS is its ability to support test software applications on both a developer's desktop and an embedded system without requiring software changes. Another important benefit of the cFS architecture is the "plug-and-play" nature of the interfaces: applications containing different functional modules (*e.g.*, navigation or maneuver planning in the case of autoNGC) can be integrated with minimal development time.

B. Navigation Filter

The navigation component uses the Goddard Enhanced Onboard Navigation System (GEONS), another flight-heritage component (dating back to 1999[16]) that has flown on several missions (*e.g.*, MMS[2, 17]) and is planned to fly on the

*https://cfs.gsfc.nasa.gov

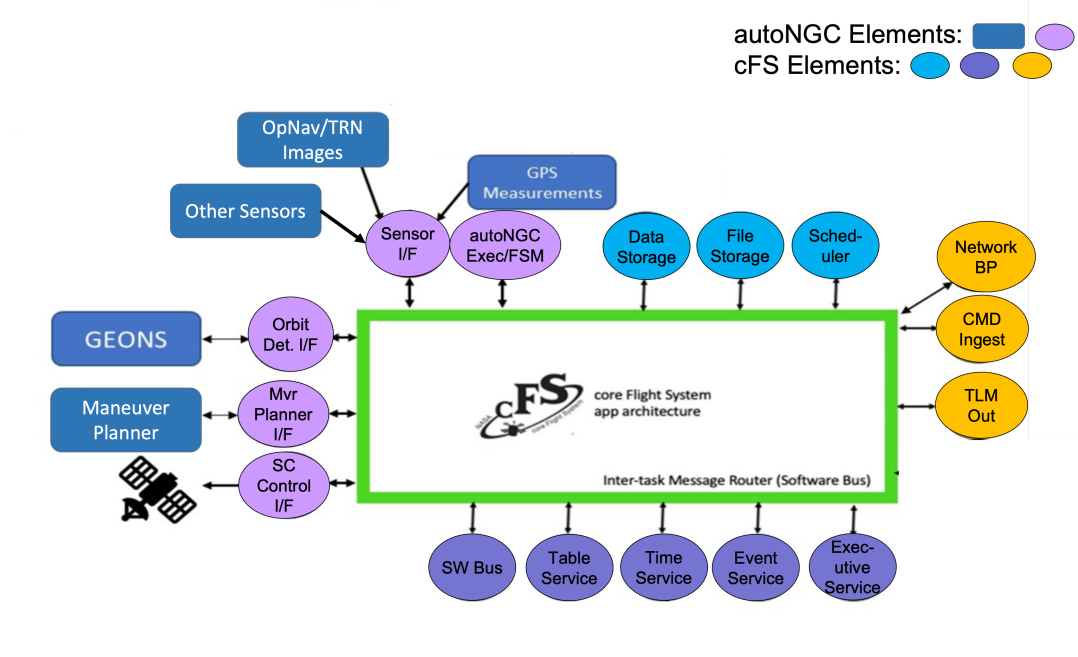

Fig. 1 Overview of autoNGC components integrated with cFS. Not all components shown here are utilized in the current simulations.

OSAM-1 mission[18]. GEONS is currently working toward a public release of version 3.0 in the near future. GEONS uses an extended Kalman filter to estimate a spacecraft's state (position and velocity) and other dynamic model parameters in real-time using onboard sensor measurements. Although not all of the following measurements are used in the present study, the GEONS system is capable of simulating and processing numerous sensors, including GNSS (GPS and Galileo) pseudorange and Doppler measurements, ground station tracking, camera-based measurements (both bearing to celestial body centers of mass or surface landmarks), laser range measurements, X-ray pulsar navigation measurements, inter-spacecraft crosslink measurements, and the ability to solve for multiple spacecraft states simultaneously. For this work, only GPS pseudorange and bearing to surface landmarks are processed.

C. Maneuver Planning

The eventual FSW capabilities of autoNGC are planned to include both a linear feedback controller and a forward shooter. The linear feedback controller produces a single control command at a given state and time and is therefore called repeatedly until a terminal target is reached, rather than producing an entire maneuver plan at once. For the lunar lander use case in this paper, a linear feedback controller based on the OSIRIS-REx touch-and-go (TAG) guidance controller was prototyped for use during the finite-burn segments that bring the vehicle close to the lunar surface. The controller produces maneuver commands that attempt to eliminate any deviations between the actual trajectory and the ground-optimized trajectory plan. autoNGC IRAD work has investigated the use of two different ground-based maneuver planning tools to develop reference trajectories for autoNGC simulations: (1) in FY2020, the Collocation Stand-Alone Library and Toolkit (CSALT)[19] was used for analysis of a lunar orbit stationkeeping use case, and (2) in FY2021, the Evolutionary Mission Trajectory Generator (EMTG)[20] was used for the current lunar lander use case. CSALT has ground-system heritage as a component of the General Mission Analysis Tool (GMAT) since 2020[21], and has been used for proposal development and future mission support on various projects at GSFC. CSALT is also currently being used by the Laser Interferometer Space Antenna (LISA) Study Office at GSFC to optimize trajectories for the ESA-led LISA mission. EMTG has been used for ground-based mission design on a number of deep-space mission applications, such as Lucy, OSIRIS-REx, and Davinci.

D. Navigation Measurement Processing

The TRN and OpNav components of autoNGC are comprised of the Retina and GIANT (Goddard Imaging Analysis and Navigation Tool) suite of software. Retina was initially developed at GSFC for the Asteroid Robotic Retrieval Mission[22], before the mission was canceled in 2017. Previous Retina software testing and technology maturation has included indoor asteroid wall testing at Lockheed Martin's Space Operations Simulation Center with algorithms running on flight-like development board processors, as well as using field data collected from aerial drones in a limestone quarry. Retina is responsible for correlating onboard *a priori* navigation maps (*i.e.*, digital terrain models (DTMs)) with real-time images from onboard sensors (*i.e.* navigation cameras), to produce line-of-sight measurements to landmarks. These small sections of the target DTMs are called "maplets", with a "landmark" representing the origin of a maplet. GIANT was originally designed to perform OpNav functions including far-field centroiding and limb-scanning of bodies[23], and has been used in the OSIRIS-REx ground system for independent navigation analysis[24] and to analyze asteroid Bennu ejecta particles[25]. The ground-system version of GIANT, written in python, is now freely available to the public as open source software[†]. Retina's TRN functionality has been merged into the FSW version of GIANT, written in C and C++, and the onboard OpNav and TRN system is now simply known collectively as cGIANT going forward.

III. Lunar Lander Use Case

This section describes a lunar lander use case for demonstrating a subset of the autoNGC functionality. This use case is not associated with any particular lunar mission in development. The purpose of this use case is to perform two separate tests of autoNGC capabilities. First is a demonstration of GEONS navigation accuracy, and second is a TRN PIL test. Both of these independent (*i.e.*, non-integrated) tests are performed for the reference lunar landing use case during descent from a low-lunar orbit (LLO) at 100-km altitude to an altitude near the surface (15 km) prior to the braking maneuver and powered descent.

The overall concept-of-operations (conops) and geometry of the orbit are designed to optimize availability of GPS and TRN measurements. The selenocentric LLO is nearly circular and highly inclined to the lunar equator. The geometry of the lunar parking orbit and descent trajectory were designed with the following goals in mind: (1) continuous availability of GPS signals at all times, (2) TRN measurement availability for a large portion of the descent trajectory. The first goal is achieved by orienting the orbit such that the orbit angular momentum vector is closely aligned to the Moon-Earth line. The second goal is achieved by selecting a landing site at fairly high northern lunar latitude and using an approach trajectory that ascends over sunlit terrain that begins when the vehicle crosses the terminator near the south pole. EMTG was used to design the reference deorbit burn and braking burns that deliver maximum mass to the surface, along with the associated reference trajectory. The orbit state and epoch were also selected to ensure that the TRN measurements occur when the terrain's local sun elevation angle is neither too low nor too high (*i.e.*, causing too much or too little surface shadowing). Shortly after the vehicle crosses the terminator, the terrain's local sun elevation angle at nadir ranges from 20 deg to 40 deg during the descent from 40 to 15 km altitude. Table 1 lists major events in the simulation, and Figure 2 is a plot showing the reference trajectory altitude history vs. time. From initialization of the simulation in the 100-km altitude LLO until the vehicle reaches 40 km altitude, only weak-signal GPS measurements are used. After the 40-km altitude point, both GPS and TRN are used. The simulation is stopped at the 15-km altitude point.

Table 1 Timeline of main simulation events.

Event	Elapsed time in simulation, hrs	Approx. lunar altitude, km
Sim start in LLO	0	100
GPS measurements start	0	100
Depart LLO with deorbit maneuver	2	100
TRN measurements start	2.6	40
Sim stop prior to braking maneuver	2.9	15

[†]https://github.com/nasa/giant

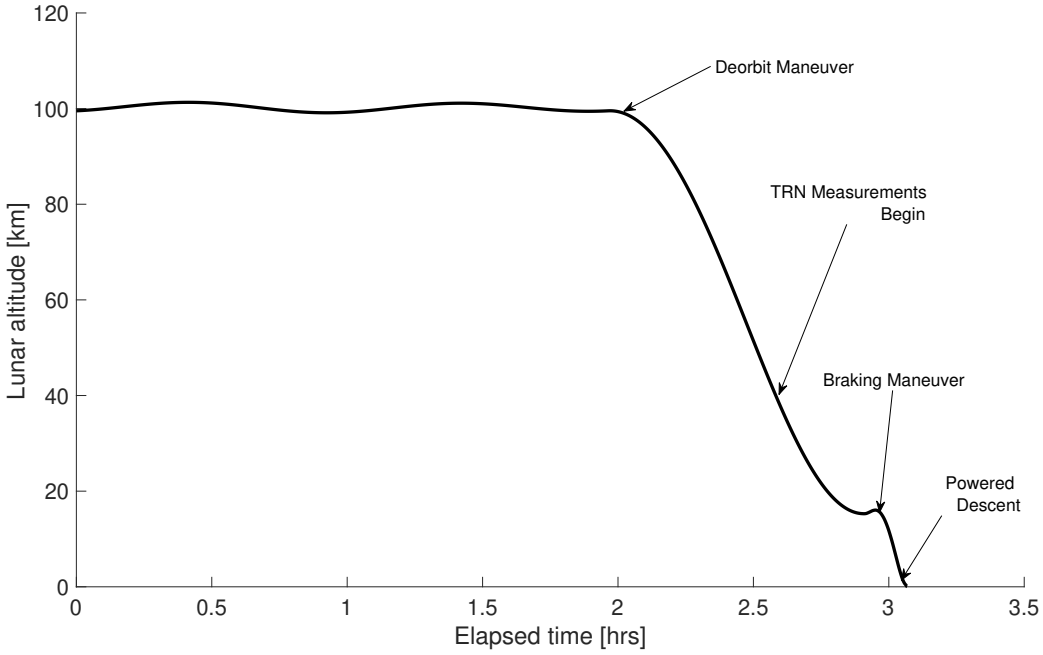

Fig. 2 Plot of reference trajectory altitude vs. time for the lunar lander use case, denoting major events.

IV. Navigation Simulations

A Matlab-based interface to GEONS is used to evaluate expected navigation accuracy over the descent trajectory shown in Figure 2. The dynamics model in both the truth and the filter assumes a point-mass lunar gravity field for this preliminary simulation; other perturbations such as solar radiation pressure and higher order gravity are disabled in the current simulation in order to minimize the modeling differences between the filter dynamics model and the model used to generate a maneuver plan. The link budget for the GPS signals assumes a 14 dB high gain Earth-pointed antenna and 23 dB-Hz acquisition threshold, per previous studies of GPS measurements in cislunar space[7]. For this use case, GPS signals are continously visible, *i.e.*, are not occulted by the Moon at any point. The initial state in the filter is randomly initialized in the parking orbit with position and velocity covariance shown in the left-most column in Table 2. The filter is first run over one revolution in the parking orbit, processing only GPS measurements, until the deorbit burn occurs at 2-hrs elapsed time into the simulation (see Figure 3). The vehicle continues processing GPS measurements, and then it crosses the terminator around 40 km altitude and TRN measurements can commence. At this point, the filter is restarted by initializing with the final state estimates and covariance from the previous run, shown in the middle column of Table 2. The TRN measurement rate is set at one surface image per minute, with 3 to 5 landmarks per image, and the measurement noise is set at 0.1 pixels 1-σ in each image pixel column/row direction. For these preliminary GEONS tests, randomly distributed surface landmarks are simulated across the surface, independent of a given truth terrain model. Figure 4 shows the navigation results as GEONS processes both GPS and TRN measurements from 40 to 15 km altitude.

Over the period of the descent when weak-signal GPS and TRN measurements are processed, we see from Figure 4 that the 3-σ position and velocity uncertainties are less than a few meters and mm/s, respectively, once the filter converges. At the final measurement time at 15 km, the final 3-σ filter uncertainties are shown in the far right column of Table 2. These uncertainties are at an encouraging level shortly prior to when the vehicle would be performing the braking maneuver, and show that it is feasible to use autonomous navigation that does not rely on DSN or other ground-based radiometric tracking. The simulations results presented here will inform the design of the terminal phase landing approach, which includes the planning of the braking maneuver and touchdown.

Table 2 GEONS filter uncertainty at initialization in LLO, restart at 40km after GPS only, and final 15km with GPS and TRN.

State	LLO Initialization 3-σ	40 km (GPS Only) 3-σ	15 km (TRN + GPS) 3-σ
Radial Position	1 km	29.6 m	1.6 m
In-track Position	1 km	24.6	0.8 m
Cross-track Position	1 km	9.6	0.6 m
Radial Velocity	1 m/s	36 mm/s	2.5 mm/s
In-track Velocity	1 m/s	15 mm/s	1.0 mm/s
Cross-track Velocity	1 m/s	5.5	1.0 mm/s

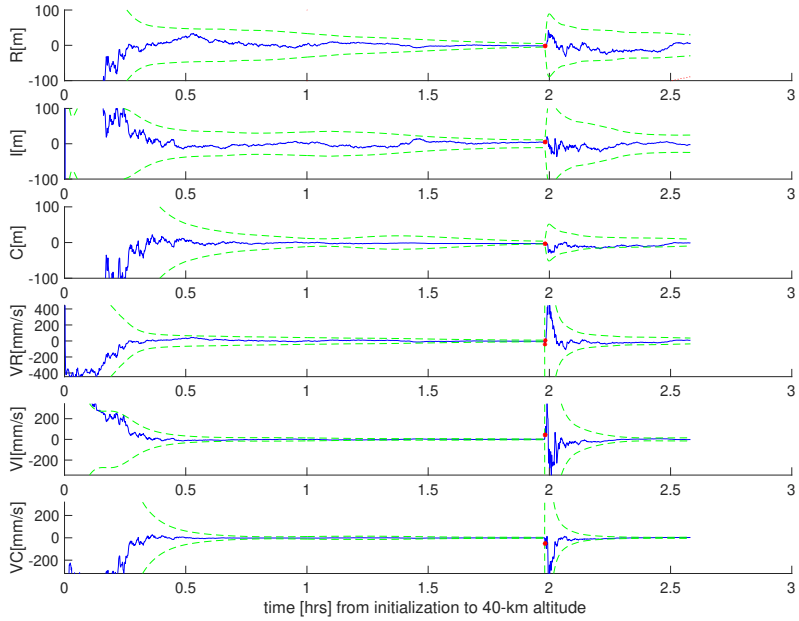

Fig. 3 GEONS navigation error RIC position and velocity components (blue) and +/- 3σ filter uncertainties (green), in selenocentric radial, in-track, cross-track components, during low lunar orbit and descent to 40 km altitude.

V. GIANT Surface Feature PIL Simulations

This section describes simulations of the GIANT image processing of surface landmarks, using synthetic images of the lunar surface. One approach to performing TRN simulations is to use synthetically generated truth terrain. Another approach is to use previously collected data from real celestial targets. The autoNGC simulations described here use real terrain products generated from the Lunar Reconnaissance Orbiter (LRO) Narrow Angle Camera (NAC). A series of python scripts was developed to process the NAC DTMs and transform these maps into the shape models needed to render both the synthetic camera images (to simulate what the onboard navigation camera "NAVCAM" would collect), as well as the navigation maplets needed by GIANT to perform TRN. The DTM processing scripts transform LRO high-resolution NAC DTMs (typically 5-m resolution), which are disjointed and spread across the lunar surface, into a semi-contiguous strip of terrain along the descent trajectory's nadir direction. The semi-contiguous strip of terrain is needed to simulate the lunar landing use case descent to 15 km altitude, which spans several hundreds of kilometers downrange. Figure 5 shows an example of a synthetic image at 40 km altitude. Note that the landmarks are defined within the NAC DTM strips, and the GIANT landmark search algorithm only needs to search within a small image area around each landmark, therefore the missing content in the image (*i.e.*, where no truth terrain is defined) is not an issue

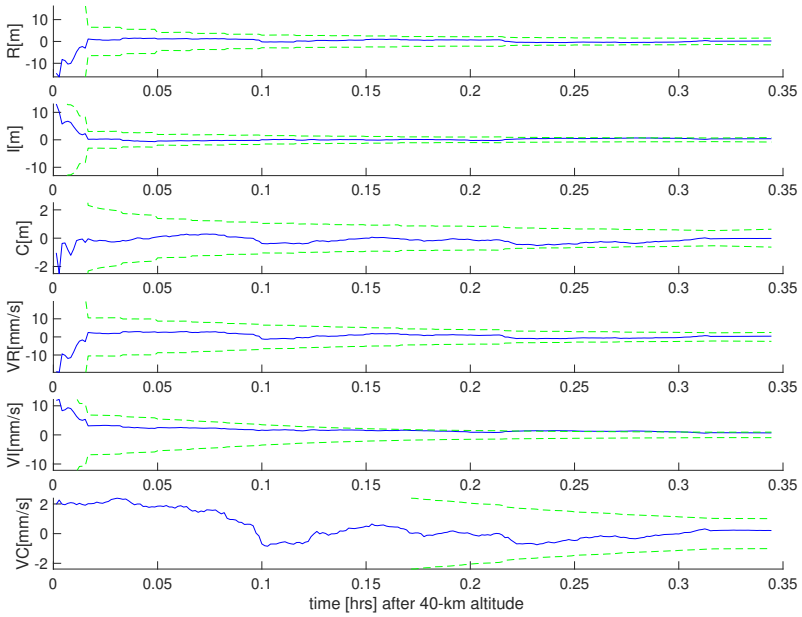

Fig. 4 GEONS navigation error RIC position and velocity components (blue) and +/- 3σ filter uncertainties (green), in selenocentric radial, in-track, cross-track components, from 40 to 15 km altitude.

for these preliminary simulations. As the vehicle approaches the surface, the NAC DTMs fill a larger fraction of the NAVCAM image, until it is nearly fully covered at 15 km altitude. Table 3 defines the NAVCAM parameters used for the current synthetic image rendering.

Table 3 NAVCAM Definition.

Parameter	Value
Detector	1440 (H) x 1080 (V) pixels
Pixel size	3.45 μm
Focal length	5.27 mm
Bits/pixel	8

The synthetic images are rendered using a custom simulation environment developed at GSFC called Freespace[26], which has supported other missions like MMS and OSAM-1. The autoNGC simulation uses the ray tracer libraries in Freespace to perform highly optimized multi-bounce ray tracing (on a central processing unit (CPU) or graphics processing unit (GPU)) to generate realistic synthetic images. We used a Lambert reflectance function to approximate the behavior of the lunar surface for these preliminary simulations, since the focus was on developing the PIL framework, as opposed to a high-fidelity evaluation of measurement accuracy.

The navigation landmarks were selected from the same high-resolution NAC DTMs used to define the truth terrain. These navigation landmarks/maplets were created by interpolating the NAC DTMs to a resolution of 8 m per grid element, which yield appropriately sized maplets given the 99×99 gridded maplet dimensions and the ground sample distance for the assumed NAVCAM over the descent. For these preliminary simulations, additional errors (such as noise or biases) were not added to the navigation maplets, beyond any small level of error caused by the interpolation. Also, GIANT is using the truth pose state relative to the terrain, in lieu of the estimated state from the filter, to establish a floor on the expected measurement accuracy.

Figure 6 shows an example of a maplet that has been rendered by GIANT's onboard algorithm, as well as the same section of the synthetic NAVCAM image of the truth terrain. In this particular example, the correlation score was 0.99

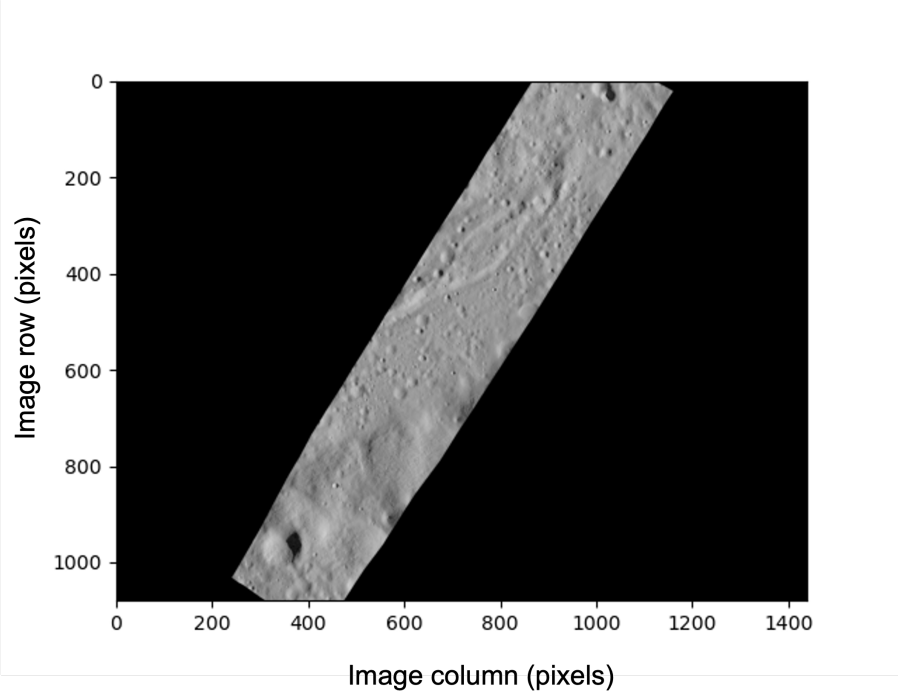

Fig. 5 Example of synthetic surface image from 40 km altitude, using a high-resolution NAC DTM. The source DTM does not fill the entire NAVCAM field-of-view at this altitude.

and the error in the measured landmark pixel coordinates were $(\text{col}, \text{row})_{\text{err}} = (-0.025, -0.169)$ pixels; we typically desire the pixel measurement error to be a fraction of pixel near zero and the correlation scores to be near 1, since no additional errors (*e.g.*, camera model, navigation maplet DTM, filter state estimate uncertainty) have been injected into the process. Figure 7 shows a 2-D distribution of landmark pixel errors over the descent trajectory from our lunar landing use case from 40 to 15 km altitude; the errors are approximately zero-mean, indicating no significant biases in the current setup. This analysis of the landmark measurement errors serves as a useful approximation of the lower-bound on the achievable measurement accuracy for lunar landmarks using this system. As more realistic error sources are included in the simulation in future tests, these pixel errors are expected to grow; the impact of higher pixels errors on navigation performance in the GEONS filter will be examined in future simulations.

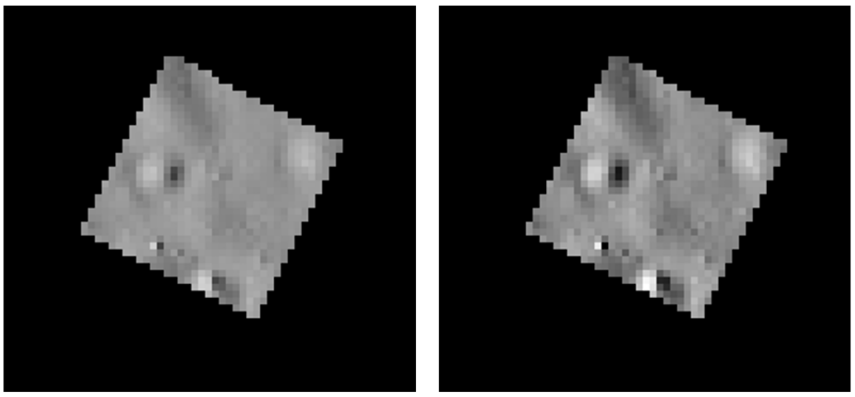

Fig. 6 (Left) navigation maplet rendered using GIANT's onboard FSW algorithms running on the PIL testbed, projected into the geometry of the NAVCAM image, (Right) corresponding image pixels in the synthetic NAVCAM image, rendered using Freespace's multi-bounce ray tracer on a workstation.

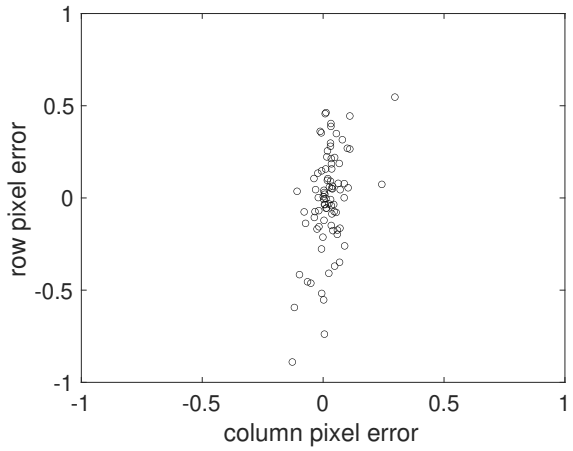

Fig. 7 Error in GIANT's measured landmark coordinates in image space during the PIL tests, expressed as image pixel column and row error.

The PIL tests were designed to evaluate autoNGC's GIANT TRN functionality and processing speeds on a flight-like processor. The autoNGC PIL testbed includes an Avnet MicroZed (AES-Z7MB-7Z020-SOM-I-G REV-G) development board with an I/O Carrier Card (Figure 8). The experiments were run on the MicroZed's 1 GHz dual-core ARM Cortex-A9 CPU included on the Xilinx Zynq-7020 FPGA with 1 GB of DDR3 SDRAM. This board was used because its Xilinx Zynq-7020 architecture makes it a suitable stand-in for the SpaceCube Mini-Z flight processor[27] and can be used to simulate the performance constraints found on the embedded platform. SpaceCube Mini-Z design is an evolution of the popular CSPv1 and features the Xilinx Zynq-7000 SoC (dual-core ARM Cortex-A9, 28-nm FPGA). This card is included on several NASA Goddard CubeSats and has extensive flight heritage.

The time to process a NAVCAM image in GIANT and generate landmark measurements depends on several factors, such as the number of landmarks, the number of image pixels contained in each maplet, the image search distance, etc. Figure 9 is a plot showing the PIL times on the development board for all of the landmarks during the descent, versus the number of image pixels contained in the maplet, *i.e.*, as the vehicle gets closer to the surface, a maplet defined with a given number of grid elements and meters per element will take up an increasing number of image pixels. For example, the maplet shown in Figure 6 is from the beginning of the TRN sequence at 40 km altitude, and takes up 823 image pixels. All of the maplets in this preliminary test have consistent definition of 99x99 grid elements, with 8 m/element, for simplicity, although future conops could explore defining navigation maplets with variable size along the reference trajectory. Figure 9 shows that processing time increases linearly with the number of image pixels contained in the maplet, which is expected given that the linear correlation computation (*i.e.*, the Pearson product moment correlation) takes up a majority of the maplet processing algorithm, and the number of calculations in this correlation increases linearly with the length of the input signal. Note that GIANT takes additional time to read in each image, and perform other calculations, beyond what is shown in Figure 9, but these computations and processing times are fairly consistent from image to image. A typical GIANT measurement generation (*i.e.*, reading in a single NAVCAM image and computing line-of-sight to five landmarks) at the beginning of our descent at 40 km takes approximately six seconds on the MicroZed board. Thus, it is clear that our numerical simulations of GEONS described above in Section IV are conservative in assuming TRN measurements that process an image once per minute with five landmarks. In practice, this means that such a lunar landing scenario can either process TRN measurements at a higher rate than what was assumed in the GEONS simulations, or can keep the rate at one image every minute and free up the onboard processor for other tasks. Note that the terminal phases of the landing trajectory (below 15 km altitude) may require more frequent maneuvers to achieve precision landing, during which time a faster TRN measurement processing time may be required. Accelerating parts of the TRN algorithm on an FPGA is one method to achieve a faster measurement processing time.

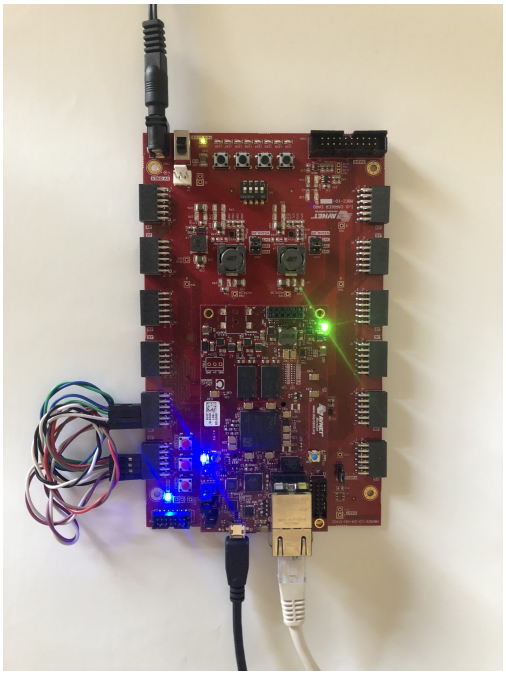

Fig. 8 Photo of the MicroZed development board used during PIL tests of autoNGC's GIANT TRN components.

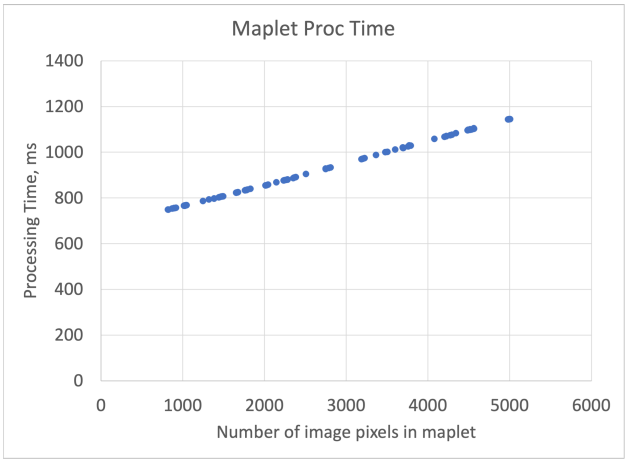

Fig. 9 Plot of PIL processor time for an individual maplet in GIANT, considering only the onboard rendering, search, and correlation steps, versus the number of image pixels contained in the maplet.

VI. Future Work

In the near future, we expect to expand upon the PIL tests described here, to include closed-loop tests of all the components described above (GEONS, GIANT, Maneuver Planning). More realistic error sources affecting the dynamics and measurements models will continue to be added, as the performance of autoNGC is evaluated for upcoming candidate missions.

VII. Conclusions

We have described the autoNGC architecture for performing autonomous navigation, guidance, and control, leveraging several NASA GSFC technologies into a cFS-based FSW system. The use case presented a transfer from a low lunar orbit into a descent trajectory down to 15-km altitude, which utilizes weak-signal GPS and TRN measurements,

to achieve position and velocity 3-σ uncertainties on the order of <2 m position and <2 mm/s velocity at the end of the sequence prior to the final braking burn. The PIL tests on a flight-like development board showed that GIANT FSW was able to process simulated surface images at a rate of approximately 6 seconds per image at 40-km altitude, with that processing time increasing linearly as the maplet image dimensions increase. These results show that autoNGC and GIANT can perform TRN at a sufficiently high measurement rate needed to support such a descent prior to the terminal landing phase.

VIII. Acknowledgements

We thank Steven Queen, Shaun Oborn, Charles Campbell, and Bryan Patrick at NASA GSFC, who led and contributed to the development of the Freespace simulation environment used in this study.

References

[1] "NASA Technology Taxonomy," `https://www.nasa.gov/sites/default/files/atoms/files/2020_nasa_technology_taxonomy_lowres.pdf`, 2021. Accessed: 2021-05-14.

[2] Winternitz, L. B., Bamford, W. A., Price, S. R., Carpenter, J. R., Long, A. C., and Farahmand, M., "Global Positioning System Navigation Above 76,000 KM for NASA'S Magnetospheric Multiscale Mission," *NAVIGATION, Journal of the Institute of Navigation*, Vol. 64, No. 2, 2017, pp. 289–300.

[3] Winternitz, L., Bamford, W., Long, A., and Hassouneh, M., "GPS Based Autonomous Navigation Study for the Lunar Gateway," *American Astronautical Society (AAS) Guidance, Navigation, and Control Conference, Breckenridge, CO*, 2019. AAS 19-096.

[4] Bamford, W., Heckler, G., Holt, G., and Moreau, M., "A GPS Receiver for Lunar Missions," *Proceedings of the 2008 National Technical Meeting of The Institute of Navigation, San Diego, CA*, 2008, pp. 268–276. AAS 19-410.

[5] Stadter, P. A., Duven, D. J., Kantsiper, B. L., Sharer, P. J., Finnegan, E. J., and Weaver, G. L., "A Weak-signal GPS Architecture for Lunar Navigation and Communication Systems," *2008 IEEE Aerospace Conference*, 2008, pp. 1–11. https://doi.org/10.1109/AERO.2008.4526347.

[6] Capuano, V., Blunt, P., Botteron, C., Tian, J., Leclère, J., Wang, Y., Basile, F., and Farine, P.-A., "Standalone GPS L1 C/A Receiver for Lunar Missions," *Sensors*, Vol. 16, No. 3, 2016. https://doi.org/10.3390/s16030347, URL https://www.mdpi.com/1424-8220/16/3/347.

[7] Ashman, B., Schlenker, L., Parker, J., Bauer, F., Winternitz, L., Long, A., Craft, K., and Hassouneh, M., "Applications and Benefits of GNSS for Lunar Exploration," *16th International Conference on Space Operations, Virtual Edition, 3-5 May*, 2021.

[8] Rutishauser, D., Epp, C., and Robertson, E., "Free-Flight Terrestrial Rocket Lander Demonstration for NASA's Autonomous Landing and Hazard Avoidance Technology (ALHAT) System," *SPACE 2012 Conference and Exposition, 11 - 13 September 2012, Pasadena, California*, AIAA, 2012. AIAA 2012-5239.

[9] Ely, T., Heyne, M., and Riedel, J., "Altair Navigation Performance During Translunar Cruise, Lunar Orbit, Descent, and Landing," *Journal of Spacecraft and Rockets*, Vol. 49, No. 2, 2012.

[10] Carson, J. M., Munk, M. M., Sostaric, R. R., Estes, J. N., Amzajerdian, F., Blair, J. B., Rutishauser, D. K., Restrepo, C. I., Dwyer-Cianciolo, A. M., Chen, G., and Tse, T., "The SPLICE Project: Continuing NASA Development of GNC Technologies for Safe and Precise Landing," *AIAA Scitech 2019 Forum*, 2019. https://doi.org/10.2514/6.2019-0660.

[11] Owens, C., Macdonald, K., Hardy, J., Lindsay, R., Redfield, M., Bloom, M., Bailey, E., Cheng, Y., Clouse, D., Villalpando, C. Y., Hambardzumyan, A., Johnson, A. E., and Horchler, A. D., "Development of a Signature-based Terrain Relative Navigation System for Precision Landing," *AIAA Scitech 2021 Forum*, 2021. https://doi.org/10.2514/6.2021-0376.

[12] Johnson, A. E., and Montgomery, J. F., "Overview of Terrain Relative Navigation Approaches for Precise Lunar Landing," *2008 IEEE Aerospace Conference*, 2008, pp. 1–10. https://doi.org/10.1109/AERO.2008.4526302.

[13] Johnson, A., Villaume, N., Umsted, C., Kourchians, A., Sternberg, D., Trawny, N., Cheng, Y., Geipel, E., and Montgomery, J., "Overview of Terrain Relative Navigation Approaches for Precise Lunar Landing," *43rd Annual AAS Guidance, Navigation and Control Conference 2020, January 30 - February 5, 2020*, 2019. AAS 20-105.

[14] Berry, K., Getzandanner, K., Moreau, M., Antreasian, P., Polit, A., Nolan, M., Enos, H., and Lauretta, D., "Revisting OSIRIS-REX Touch-And-Go(TAG) Performance Given the Realities of Asteroid Bennu," *AAS Guidance, Navigation and Control Conference, Jan. 30, 2020*, 2020. AAS 20-088.

[15] McComas, D., Wilmot, J., and Cudmore, A., "The Core Flight System (cFS) Community: Providing Low Cost Solutions for Small Spacecraft," *30th AIAA/USU Conference on Small Satellites*, AIAA, 2016. SSC16-IV-1.

[16] Gramling, C., Lorah, J., Santoro, E., Work, K., and Chambers, R., "Preliminary Operational Results of the TDRSS Onboard Navigation System (TONS) for the Terra Mission," https://ntrs.nasa.gov/citations/20000092085, 2000. Accessed: 2021-11-16.

[17] Farahmand, M., Long, A., and Carpenter, R., "Magnetospheric MultiScale Mission Navigation Performance Using the Goddard Enhanced Onboard Navigation System," *Proceedings of the 25th International Symposium on Space Flight Dynamics*, 2015.

[18] Vavrina, M., Skelton, E., DeWeese, K., Naasz, B., Gaylor, D., and D'Souza, C., "Safe Rendezvous Trajectory Design for the Restore-L Mission," *Advances in the Astronautical Sciences*, 2019. AAS 19-410.

[19] Hughes, S., Knittel, J., Shoan, W., Kim, Y., Conway, C., and Conway, D., "Benchmarking the Collocation Stand-ALone Library and Toolkit (CSALT)," *Proceedings of the 26th International Symposium on Space Flight Dynamics*, 2017.

[20] Englander, J., Ellison, D., Williams, K., McAdams, J., Knittel, J., Sutter, B., Welch, C., Stanbridge, D., and Berry, K., "Optimization of the Lucy Interplanetary Trajectory via Two-Point Direct Shooting," *Advances in the Astronautical Sciences, Spaceflight Mechanics*, Vol. 171, 2019. AAS 19-663.

[21] "General Mission Analysis Toolkit," https://gmatcentral.org, 2021. Accessed: 2021-05-14.

[22] Shoemaker, M. A., Wright, C., Liounis, A., Getzandanner, K. M., Van Eepoel, J. M., and DeWeese, K. D., "Performance Characterization for a Landmark Measurement System for ARRM Terrain Relative Navigation," *Advances in the Astronautical Sciences, Spaceflight Mechanics*, Vol. 158, 2016. AAS 16-286.

[23] Wright, C., Liounis, A., and Ashman, B., "Optical Navigation Algorithm Performance," *1st Annual RPI Workshop on Image-Based Modeling and Navigation for Space Applications, Troy, NY*, 2018.

[24] Liounis, A. J., Swenson, J. C., Small, J., Lyzhoft, J., Ashman, B. W., Getzandanner, K. M., and Lauretta, D. S., "Independent Optical Navigation Processing for the OSIRIS-REx Mission Using the Goddard Image Analysis and Navigation Tool," *2nd RPI Workshop on Image-Based Modeling and Navigation for Space Applications, Troy, NY*, 2019.

[25] Liounis, A., Small, J., Swenson, J., Lyzhoft, J., Ashman, B., Getzandanner, K., Moreau, M., Adam, C., Leonard, J., Nelson, D., Pelgrift, J., Bos, B., Chesley, S., Hergenrother, C., and Lauretta, D., "Autonomous Detection of Particles and Tracks in Optical Images," *Earth and Space Science*, Vol. 7, No. 8, 2020.

[26] Queen, S., Shah, N., and Benegalrao, S., "Generalized Momentum Control of the Spin-Stabilized Magnetospheric Multiscale Formation," *Advances in the Astronautical Sciences, Spaceflight Mechanics*, Vol. 156, 2015. AAS 15-816.

[27] Brewer, C., Franconi, N., Ripley, R., Geist, A., Wise, T., Sabogal, S., Crum, G., Heyward, S., and Wilson, C., "NASA SpaceCube Intelligent Multi-Purpose System for Enabling Remote Sensing, Communication, and Navigation in Mission Architectures," *34th Small Satellite Conference, Utah State University*, 2020. SSC20-VI-07.